INSIGHTS INTO CIRCUM-THARSIS WRINKLE RIDGES. O. Karagoz[1], T. Kenkmann[1] and G. Wulf [1], [1]Institute of Earth and Environmental Sciences (Geology), Albert-Ludwigs-University Freiburg, Germany.

Introduction: Wrinkle ridges are curvilinear, broad arched, and superposed double ridge morphologies [1], and most of them occur, where horizontal shortening is dominant [2]–[4]. On Mars, the Tharsis bulge is an example of a large igneous province that results in a contractional stress regime in its periphery [5]–[7]. The morphologies of circum-Tharsis wrinkle ridges can vary to a large extent due to complex subsurface fault patterns and varying material properties [7]–[9]. Likewise their physical dimensions [8]–[12], and the amount of horizontal shortening varies considerably (e.g., [13]–[15]). A number of conceptual models (e.g., [1], [13], [16]–[19]) of wrinkle ridge formation has been proposed. Shortening in these models is accommodated by either buckling or thrust/reverse faulting (thick-skinned tectonic models). Other models interpret wrinkle ridges as fault-bend folds or fault propagation folds and propose a detachment at depth (thin-skinned tectonic models)[13], [14], [17], [20], [21]. Despite the rather extensive research on wrinkle ridges, we aim to perform a detailed morphometrical analysis of the wrinkle ridges making use of high-resolution remote sensing data, to test a kinematic model of wrinkle ridge formation that is directly linked to measurable morphometric parameters and provides information on the amount of shortening, the depth of detachment, and ramp angle. We use methods that were developed to analyze the tectonics of fold-and-thrust belts on Earth to construct balanced cross-sections of the wrinkle ridges. We assume that wrinkle ridge formation postdates volcanic activity in that region. Our balancing approach conserves area and volume and keeps the thicknesses of strata constant during deformation.

Methodology: In order to perform a detailed morphometric analysis on wrinkle ridges, we had to identify suitable wrinkle ridges that are covered by high-resolution remote sensing data. We have chosen 6 wrinkle ridges (WR) at Lunae Planum that show representative morphology, minor signs of erosion, and traceable signs of faulting (Fig 1a). We produced high-resolution digital elevation models (DEMs) based on CTX images by using the Ames Stereo Pipeline [22] in combination with the Integrated System for Imagers and Spectrometers (ISIS) software [23].

The crest lines of the wrinkle ridges were mapped as linear datasets in 2 km segments with respect to position, length, and orientation. We produced a MATLAB script that automatically analyzes the wrinkle ridges using more than 500 elevation profiles perpendicular to crestline of ridges. The orientations of the wrinkle ridge segments were used to characterize their trend with respect to the Tharsis Dome (111.08°N, 9.38°E) and to evaluate whether the wrinkle ridges are formed concentrically or not. Cross-sectional area, width and mean height of the wrinkle ridges were automatically calculated based on trapezoidal numerical integration, and determination of the second derivative of the elevation change in the topographic profiles, respectively. In addition, we used CTX-DEMs to measure a few dips of fault planes underneath wrinkle ridges. This was possible, e.g. where the steep slopes of Kasei Valles [71,17°W, 20,57°N] and an impact crater

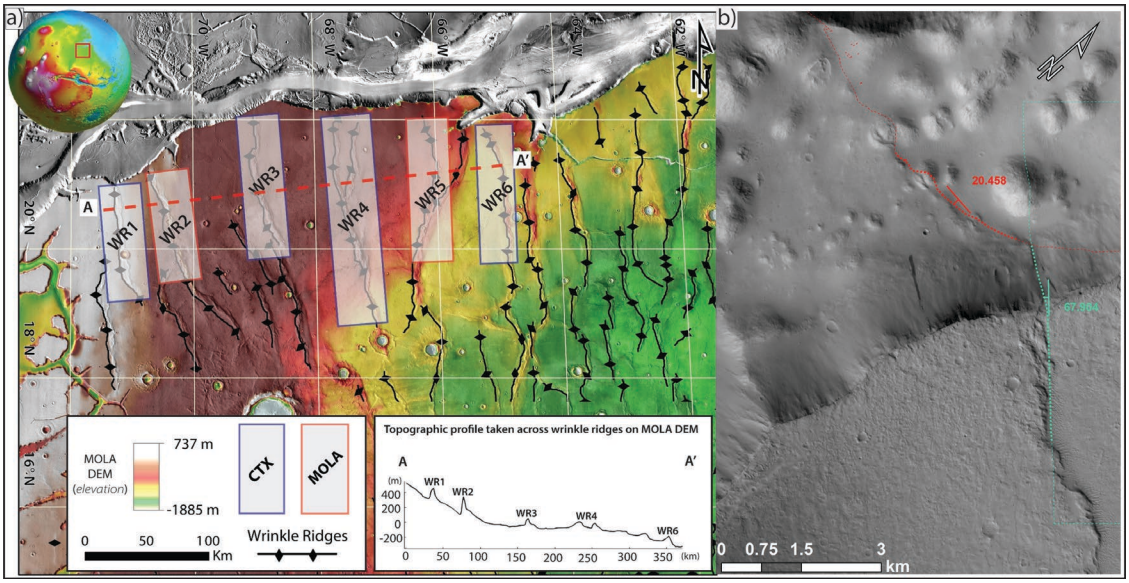

Figure 1. a) The color-as-height MOLA DEM showing the location of the examined wrinkle ridges WR1- WR6. Wrinkle ridge landforms are covered by either CTX or MOLA imagery products. The inlet topographic profile (from MOLA DEM) indicates a generally decreasing trend in elevation from west to east. b) A relatively fresh reverse fault shows a distinct kink point at a depth of roughly 850 m below the surface.

[71,7°W, 19,57°N] expose the subsurface of a wrinkle ridge.

We used the fault-propagation model of Suppe and Medwedeff [24], [25] to link the measurable wrinkle ridge height, width, and area with the amount of shortening, ramp angle and the depth of the detachment. The fold keeps shape and position relative to the propagating fault tip but grows in size by beds rolling through kink-band boundaries and fault bending [24]. To simplify our approach, we used a constant layer thickness and considered a horizontal detachment ($\Theta 1 = 0$) as a boundary condition [19].

Results: Wrinkle ridges on Lunae Planum are oriented predominantly concentrically with respect to the Tharsis rise center [19]. The majority of segments are trending 160–180° with a deviation of 10–20°. The average result of the linear regression method of morphometric analyses is $R^2 = 0.74$. The maximum height, mean height, width, and the area underneath wrinkle ridge profiles decreases from west (WR1) to east (WR6) with increasing radial range from the Tharsis center. Local exposures of thrust faults underneath wrinkle ridges dip with 38° ± 5°. We model wrinkle ridges as fault-propagation folds and show that the observed thrust faults form along the frontal fold axial planes of the anticlines. At depth these faults merge into more gentle thrust ramps of 20° ± 5° dip. Kinematic modeling of fault propagation folding was used to balance the uplifted area of wrinkle ridges. It indicates that the amount of horizontal shortening decreases from ~116 m in the west (WR1) to ~56 m in the east (WR6) with increasing distance from the Tharsis center while the depth of the detachment rises gently from 4 km depth in the west to about 2.6 km in the east, measured from the surface.

Discussion: The development of the massive volcanic Tharsis province caused flexural loading of the lithosphere and induced horizontal compressive stresses in the periphery of the province. The eastward descending topography of Lunae Planum (Fig. 1a) and the eastward rising detachment define a narrow wedge that is considered as an incipient critical taper with a tectonic push from the Tharsis center [19]. This horizontal push leads to shortening in the form of concentrically striking wrinkle ridges. In this study, our maximum shortening amount is coherent with a previously suggested amount of horizontal shortening at Lunae Planum, which is ~131 m [13], [15]. However, early conceptual models [13]– [15], [17], [18], [20] and our approach [19] use simplified geometries and neglect some complexities that characterize wrinkle ridges such as the observed changes in slope and polarity, bifurcation of wrinkle ridges, or the numerous faults that are responsible for their wrinkly appearance. To decipher the ground-truth structure of wrinkle ridges at depth, three-dimensional exposures of wrinkle ridges are necessary. We have identified a number of circum-Tharsis wrinkle ridges that provide at least partial insights into the subsurface structure. Key outcrops are where wrinkle ridges are cut by impact craters. The first inspection of such localities indicates that reverse faults are situated beneath the steeper flanks of wrinkle ridges. The reverse faults show a distinct kink point at a depth of roughly 850 m below the surface and continue as shallowly dipping thrust faults at greater depth (Fig 1b). Abundant secondary faults are associated with the main fault. Antithetic subsidiary faults along with the main reverse fault may transit into symmetric conjugate fault systems along strike of the wrinkle ridge. If the displacement on the antithetic fault becomes dominant a polarity change in the morphology of the wrinkle ridge is the consequence.

Acknowledgments: This work was supported by a scholarship grant of the Deutscher Akademischer Austauschdienst (DAAD). The used image data are available in the Planetary Data System at https://pds-imaging.jpl.nasa.gov/volumes/mro.html (License: U.S. Government Works).

References:

[1] Andrews-Hanna J.C. (2020) *Icarus*, 351,113937. [2] Scott D. H. and Tanaka K. L. (1986) *USGS,*1802. [3] Strom R. G. et al. (1975) *JGR*, 80, 2478–2507. [4] Kreslavsky M. A. and Basilevsky A. T. (1998) *JGR*, 103, 11103–11111. [5] Banerdt, W. B. et al. (1992) Stress and tectonics on Mars. [6] Mège D. and Reidel, S. P. (2001) *Geophys. Res. Lett*., 28, 3545–3548. [7] V.L. Sharpton and J. W. Head (1988) LPS XVIII, Abstract#307. [8] Plescia J. B. and Golombek M. P (1986) *Bull. Geol. Soc. Am*., 97, 1289–1299. [9] Strom R. G. (1972), Dordrecht: Springer Netherlands, 187–215. [10] Mueller K. and Golombek M. (2004) *Annu. Rev. Earth Planet. Sci.*, 32, 435–464. [11] Watters T. R. and Robinson M. S. (1997) *JGR Planets*, 102,10889–10903. [12] Golombek M. P. and Phillips R. J (2010) Eds. Cambridge University Press,183–232. [13] Golombek, M. P. et al. (1991) *LPS XXI*, Abstract#679. [14] Mangold N. et al. (1998) *Planet. Space Sci*., 46, 345–356. [15] Plescia J. B. (1991) *Geophys. Res. Lett.*, 18, 913–916. [16] Montési L. G. J. and Zuber M. T. (2003) *JGR Solid Earth*, 108,1–16. [17] Schultz R. A. (2000) *JGR Planets*, 105, 12035–12052. [18] Watters T. R. (2004), *Icarus*, 171, 284–294. [19] Karagoz O. et al. (2022) *Icarus*, 374,114808. [20] Allemand P. and Thomas P. G. (1995) *JGR*, 100, 3251. [21] Zuber M. T. and Aist L. L. (1990) *JGR*, 95, 215-230. [22] Moratto Z. M. et al. (2010) *LPSC XLI*, Abstract#2364. [23] Becker, K. ~J. et al. (2013) *LPSC XLIV*, Abstract#2829. [24] Suppe J. and Medwedeff D. A. (1990) *Eclogae Geol. Helv*., 83, 409–454. [25] Suppe J. and Medwedeff D. A. (1984) *GSA* 16, Abstract#670.